Available online at www.sciencedirect.com
ScienceDirect
Trans. Nonferrous Met. Soc. China 31(2021) 2740−2749
Transactions of Nonferrous Metals Society of China
www.tnmsc.cn

Structure, mechanical and thermal properties of Y-doped CrAlN coatings

Jin-lian TIAN[1], Chun HU[1], Li CHEN[1], Yu-min LOU[2], Ning-ning ZHAO[2]

1. State Key Laboratory of Powder Metallurgy, Central South University, Changsha 410083, China;
2. Zhejiang Energy Group R&D Institute Co., Ltd., Hangzhou 412007, China

Received 5 October 2020; accepted 18 February 2021

Abstract: CrAlYN coatings with different Y contents (0, 5 and 12 at.%) were deposited by cathodic arc evaporation to investigate the influence of Y-addition on the structure, mechanical and thermal properties of CrAlN coatings by using X-ray diffraction, scanning electron microscopy, differential scanning calorimetry, thermal gravimetric analysis and nanoindentation. The structural transformation of single phase cubic $Cr_{0.42}Al_{0.58}N$ and $Cr_{0.39}Al_{0.56}Y_{0.05}N$ coatings to cubic−wurtzite mixed $Cr_{0.32}Al_{0.56}Y_{0.12}N$ coating leads to a drop in hardness from (30.2±0.7) GPa of $Cr_{0.42}Al_{0.58}N$ and (32.0±1.0) GPa of $Cr_{0.39}Al_{0.56}Y_{0.05}N$ to (25.2±0.7) GPa of $Cr_{0.32}Al_{0.56}Y_{0.12}N$. The incorporation of 5 at.% Y retards the thermal decomposition of CrAlN, verified by the postponed precipitation of *w*-AlN and N-loss upon annealing. Correspondingly, $Cr_{0.39}Al_{0.56}Y_{0.05}N$ coating consistently exhibits the highest hardness value during thermal annealing. Nevertheless, alloying with Y exerts an adverse effect on the oxidation resistance of CrAlN.

Key words: CrAlYN coatings; cathodic arc evaporation; structural evolution; hardness; thermal stability; oxidation resistance

1 Introduction

Transition metal nitrides have been widely used as protective coatings for tools, dies and components owing to their high hardness, superior oxidation resistance, excellent tribological properties and promising corrosion resistance [1−4]. Amongst them, CrAlN coatings deposited by physical vapor deposition (PVD) have gained extensive attention as a promising type of wear-resistant hard coatings. CrAlN coatings are developed by incorporating Al atoms into CrN lattices, replacing a part of the Cr atoms to form a metastable substitutional solid solution with superior mechanical properties [5]. Besides, CrAlN coatings reveal exceptional oxidation resistance as a dense and protective $(Al,Cr)_2O_3$ oxide layer is formed in the early stage of oxidation inhibiting O^{2-} from diffusing inward [6]. Nevertheless, the high-temperature applications of CrAlN coatings are still limited due to their relatively inferior thermal stability, for which their hardness reveals a dramatic downtrend after the temperature exceeding 900 °C. Under exposure to high temperatures, CrAlN coatings undergo thermal decomposition in two forms. For one thing, the metastable *c*-AlN transforms into its stable phase wurtzite (*w*-) AlN with low hardness. For another, the unstable Cr—N bonds break and Cr with body-centered cubic (bcc) structure is formed via an intermediate phase hexagonal (*h*-) Cr_2N [7].

To further improve the comprehensive properties of CrAlN coatings, alloying with the fourth element (V [8], Ta [9], Zr [10], Si [11] and B [12], etc) has been developed as an effective method due to its potential to retard the diffusion-involved processes like recovery, decomposition and recrystallization. Among them, V-addition effectively enhances the thermal stability of CrAlN

Corresponding author: Li CHEN, Tel: +86-13975870633, E-mail: chenli_927@126.com
DOI: 10.1016/S1003-6326(21)65689-3
1003-6326/© 2021 The Nonferrous Metals Society of China. Published by Elsevier Ltd & Science Press

coatings by suppressing the formation of *w*-AlN and the dissociation of Cr—N bonds [13]. Besides, V-addition reduces the friction coefficient at high temperatures on account of the formation of lubricious oxides in CrAlVN coatings [14]. Adding moderate Ta is found to improve the thermal stability and mechanical properties of CrAlN coatings [9]. Zr-alloyed CrAlN coatings show excellent high temperature tribological properties for the formation of a Cr_2O_3-rich layer that reduces friction coefficient and wear rate [15]. Si-doped CrAlN coatings with nanocomposite structure obtain not only superior oxidation resistance but also improved corrosion resistance [16,17]. Alloying with B brings about a significant enhancement in mechanical properties and oxidation resistance compared with CrAlN coatings [18].

Apart from the mentioned alloying elements above, Y-incorporation has gained great attention in recent years as it significantly enhances the oxidation resistance of CrAlN coatings [19,20]. The segregation of yttrium atoms at grain boundaries and the formation of Al-rich oxide layers block the diffusion of cations (especially Cr ions) and anions, thus perfecting the oxidation resistance of CrAlN coatings [20]. There are also some reports on the mechanical properties [21] and thermal stability [22] of CrAlYN coatings. The hardness of CrAlN coatings is increased by alloying with a small amount of Y owing to solid solution mechanism and Hall−Petch effect [20]. In terms of thermal stability, incorporation of yttrium into CrAlN coating effectively retards the diffusion-associated processes [22]. Hence, Y-addition at a suitable amount is a feasible approach to improve the hardness, oxidation resistance and thermal stability of CrAlN coatings.

At present, the studies are mainly focused on CrAlYN coatings with a low content of yttrium (around 1 at.%) [19,20,23,24], while there are less systematic studies involving the performances of CrAlYN coatings with higher yttrium contents. In addition, the detailed phase evolution during the oxidation process of CrAlYN coatings, which is vital to ascertain the mechanism of Y tailoring the oxidation resistance of CrAlN coatings, has not been investigated before. Therefore, CrAlYN coatings with a wide range of Y contents (0, 5 and 12 at.%) were prepared in this work to investigate their structure, mechanical properties, oxidation resistance and thermal stability.

2 Experimental

2.1 Coating depositions

CrAlN and CrAlYN coatings were deposited on various substrates in a set of commercial equipment (Oerlikon Balzers RCS) by cathodic arc evaporation using $Cr_{0.40}Al_{0.60}$, $Cr_{0.35}Al_{0.60}Y_{0.05}$, and $Cr_{0.30}Al_{0.60}Y_{0.10}$ (99.99% in purity) targets, respectively. The used substrates include cemented carbides (WC−6wt.%Co), steel foils, tungsten (W) plates, and polycrystalline Al_2O_3 sheets, varying with the determination methods. To enhance the adhesion between substrate and coating, the substrates were ultrasonically cleaned in ethanol. Before deposition, the chamber was vacuumed to a pressure lower than 1.0×10^{-3} Pa and heated to 550 °C. Subsequently, an argon discharging process was conducted for 30 min to clean the substrates with a target−substrate distance of 240 mm. Afterward, coatings were deposited under a nitrogen (N_2, 99.99% in purity) atmosphere at approximately 3.0 Pa with a target current of 140 A and a bias voltage of −40 V.

2.2 Post-deposition treatments

Prior to thermal treatments, the coated low-alloying steel foils were dissolved in nitric acid to separate substrates and coatings. Then, the obtained flakelets of coatings were ground into powder. To study the thermal stability of coatings, the obtained powder samples were placed in a differential scanning calorimetry (DSC) instrument (Netzch STA 409C) under a pure Ar atmosphere and gradually heated up from room temperature (RT) to a specific annealing temperature (T_a=900, 1000, 1100, 1200, 1300, 1450 and 1550 °C) with a heating rate of 10 °C/min. Afterward, they were cooled down at a rate of 50 K/min. Besides, the samples onto W plates were placed in a vacuum furnace (COD533R, pressure ≤10^{-3} Pa) for vacuum annealing. The furnace was heated to a specific temperature (T_a=800−1100 °C) with a heating rate of 10 °C/min for heat preservation of 30 min. Finally, the samples were naturally cooled down to RT with furnace cooling.

Synchronous DSC and thermal gravimetric analysis (TGA) experiments in flowing synthetic air

(79 vol.% N_2, 21 vol.% O_2, 20 mL/min) were performed to measure the heat flow and mass change on the same thermal analysis instrument from RT to 1500 °C with a heating rate of 10 °C/min and a cooling rate of 50 °C/min. The isolation oxidation experiments of coated poly-crystalline Al_2O_3 substrates were performed in a DSC instrument at 800 °C for 15 h in synthetic air.

2.3 Characterizations

The surface and fracture cross-sectional morphologies of as-deposited and oxidized samples were investigated by scanning electron microscope (SEM, Zeiss Supra 55). The compositions of as-deposited coatings were determined by an energy-dispersive X-ray spectroscopy (EDX, Oxford Instrument X-MaX) detector attached to SEM. The crystal structure of specimens in various states was examined by X-ray diffraction (XRD), using a Bruker D8 Advance diffractometer in the Bragg−Brentano configuration with Cu K_α source (λ=1.541 Å). Hardness (H) and elastic modulus (E) measurements of coated W specimens were carried out with a nanoindentation instrument (Anton Paar UNHT³) with a Berkovich diamond tip following the Oliver−Pharr method [25]. A penetration load of 15 mN can ensure that the indentation depth (~160 nm) is less than 10% of the coating thickness, avoiding the interference of substrates. Average values and standard deviations were obtained from at least 20 indents.

3 Results and discussion

3.1 Chemical composition, structure, and morphology

Based on EDX measurements, the prepared CrAlN and CrAlYN coatings are stoichiometric as they present a nitrogen content of ~50 at.%. Their nominal compositions are $Cr_{0.42}Al_{0.58}N$, $Cr_{0.39}Al_{0.56}Y_{0.05}N$ and $Cr_{0.32}Al_{0.56}Y_{0.12}N$, corresponding to $Cr_{0.40}Al_{0.60}$, $Cr_{0.35}Al_{0.60}Y_{0.05}$ and $Cr_{0.30}Al_{0.60}Y_{0.10}$ targets, respectively. The composition deviations between coatings and the counterpart targets are ascribed to the different atomic evaporation rates of each element, the scattering and re-sputtering process [26]. Figure 1 presents the XRD patterns of as-deposited coatings. $Cr_{0.42}Al_{0.58}N$ and $Cr_{0.39}Al_{0.56}Y_{0.05}N$ coatings present a single phase face-centered cubic (fcc) structure. $Cr_{0.32}Al_{0.56}Y_{0.12}N$ coating exhibits a mixed structure of cubic and wurtzite, as better observed in the XRD pattern of fine scanning in the inset of Fig. 1, indicating that Y-incorporation decreases the metastable solubility limitation of c-AlN in Cr—N. Atomic radius of Y (1.80 Å) [27] is larger than that of Cr (1.40 Å) [27] or Al (1.25 Å) [27], leading to the expansion of CrAlN lattice and an increase of lattice parameter [28] from (4.1072±0.0015) Å ($Cr_{0.42}Al_{0.58}N$) to (4.1594±0.0009) Å ($Cr_{0.39}Al_{0.56}Y_{0.05}N$), and then to (4.1938±0.0105) Å ($Cr_{0.32}Al_{0.56}Y_{0.12}N$). The XRD peaks shift to lower 2θ diffraction angles with increasing Y content, further verifying the lattice expansion by Bragg's law. Besides, alloying with 12 at.% Y causes an obvious widening of the diffraction peaks, indicating the decreased grain size of $Cr_{0.32}Al_{0.56}Y_{0.12}N$ coating. The mean crystallite sizes of ~327 nm for $Cr_{0.42}Al_{0.58}N$, ~134 nm for $Cr_{0.39}Al_{0.56}Y_{0.05}N$ and ~5 nm for $Cr_{0.32}Al_{0.56}Y_{0.12}N$ are roughly calculated using the Scherrer equation [29].

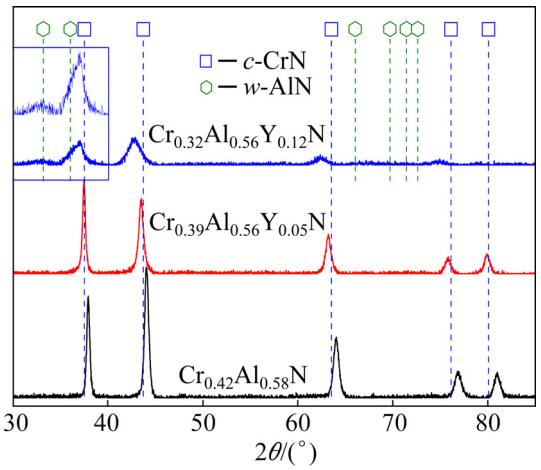

Fig. 1 XRD patterns of as-deposited $Cr_{0.42}Al_{0.58}N$, $Cr_{0.39}Al_{0.56}Y_{0.05}N$ and $Cr_{0.32}Al_{0.56}Y_{0.12}N$ coatings

Figure 2 displays SEM surface and fracture cross-sectional morphologies of CrAlN and CrAlYN coatings. All coatings present defects derived from the evaporation of target macro-particles with different melting points during evaporation process. PANJAN et al [30] reported that cathode materials with a low melting point can give rise to larger droplets, which explains the phenomenon that the droplet size of Y-alloying coatings is increased. The fracture cross-sections convey that the thickness of all coatings is ~3.0 μm. $Cr_{0.42}Al_{0.58}N$ (Fig. 2(d)) exhibits a typically dense

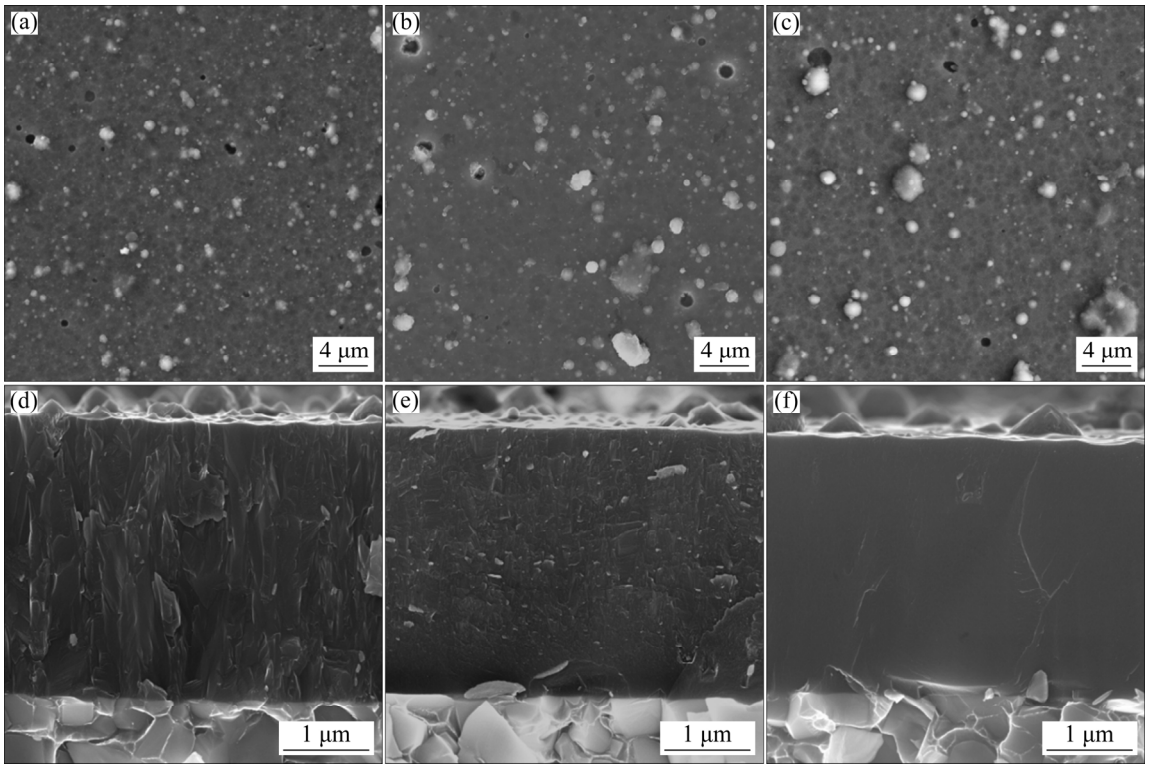

Fig. 2 SEM surface (a−c) and fracture cross-sectional (d−f) morphologies of as-deposited $Cr_{0.42}Al_{0.58}N$ (a, d), $Cr_{0.39}Al_{0.56}Y_{0.05}N$ (b, e), and $Cr_{0.32}Al_{0.56}Y_{0.12}N$ (c, f) coatings

and columnar crystal morphology. Doping with Y hinders the growth of the columnar crystal and leads to the grain refinement. $Cr_{0.39}Al_{0.56}Y_{0.05}N$ (Fig. 2(e)) shows a fine columnar structure. As Y content increases to 12 at.%, obvious grain refinement and nanocrystalline morphology of $Cr_{0.32}Al_{0.56}Y_{0.12}N$ are observed, as shown in Fig. 2(f). The grain refinement of $Cr_{0.39}Al_{0.56}Y_{0.05}N$ coating stems from the strain induced by lattice expansion. And the nanocrystalline morphology of $Cr_{0.32}Al_{0.56}Y_{0.12}N$ coating is related to the competitive growth of cubic and wurtzite phases, which dramatically constrains the growth of columnar crystal. Moreover, the formation of wurtzite phase provides plenty of nucleation sites [31], which also contributes to the formation of nanocrystalline morphology.

3.2 Mechanical properties

Figure 3 depicts the nanoindentation hardness and elastic modulus of CrAlN and CrAlYN coatings. The hardness of $Cr_{0.39}Al_{0.56}Y_{0.05}N$ rises to (32.0±1.0) GPa due to the solution strengthening and Hall−Petch effect (grain refinement) [20,32], compared to a hardness of (30.2±0.7) GPa of the

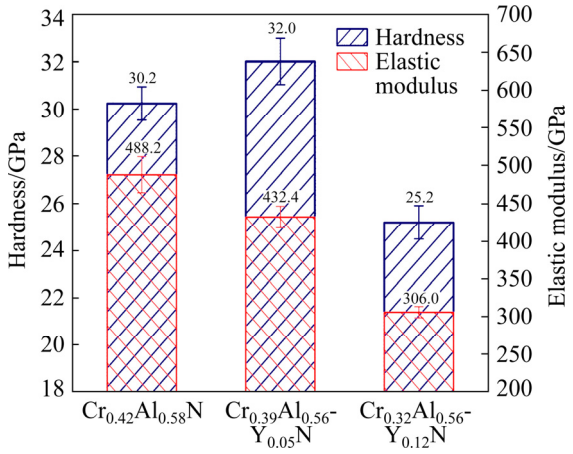

Fig. 3 Nanoindentation hardness and elastic modulus of as-deposited $Cr_{0.42}Al_{0.58}N$, $Cr_{0.39}Al_{0.56}Y_{0.05}N$, and $Cr_{0.32}Al_{0.56}Y_{0.12}N$ coatings

$Cr_{0.42}Al_{0.58}N$. However, the hardness of $Cr_{0.32}Al_{0.56}Y_{0.12}N$ coating decreases to (25.2±0.7) GPa due to the formation of *w*-AlN. As mentioned above, doping with yttrium gives rise to the decrease of grain size. KIM and BUSH [33] reported that grain refinement could contribute to a reduction of elastic modulus. Thus, the elastic modulus decreases from (488.2±23.6) GPa of $Cr_{0.42}Al_{0.58}N$ to (432.4±14.2) GPa of $Cr_{0.39}Al_{0.56}Y_{0.05}N$. In addition,

the formation of *w*-AlN leads to a further deduction in elastic modulus of $Cr_{0.32}Al_{0.56}Y_{0.12}N$ to (306.0±7.6) GPa with the combined effect of grain refinement [33].

3.3 Thermal stability

To investigate the impact of Y-addition on the structural evolution of CrAlN coatings during annealing, XRD determinations were performed for $Cr_{0.42}Al_{0.58}N$, $Cr_{0.39}Al_{0.56}Y_{0.05}N$, and $Cr_{0.32}Al_{0.56}Y_{0.12}N$ coatings annealed at given temperatures, as shown in Fig. 4. After annealing at 900 °C, $Cr_{0.42}Al_{0.58}N$ coating maintains its original single-phase fcc structure with a slight shift of peaks to a higher diffraction angle, which is associated with the recovery process involving stress relaxation and the annihilation of defects [34]. As the annealing temperature (T_a) increases to 1000 °C, a weak diffraction peak of *w*-AlN at 2θ=~33.2° is observed. After annealing at T_a=1100 °C, *h*-Cr_2N, which is the product of Cr—N dissociation [35], is detected at 2θ=~37.3°, 40.2° and 42.6°. With increasing T_a to 1200 °C, the continuous thermal decomposition leads to elevated diffraction intensities of *w*-AlN and *h*-Cr_2N. And bcc-Cr is formed due to the further dissociation of Cr—N bonds of *h*-Cr_2N at 1200 °C. Besides, the original peaks of *c*-(Cr,Al)N can hardly be detected. At 1450 °C, the N-loss process terminates and the *h*-Cr_2N has fully transformed into bcc-Cr. Finally, $Cr_{0.42}Al_{0.58}N$ completely decomposes into *w*-AlN and bcc-Cr at 1550 °C.

On the other side, $Cr_{0.39}Al_{0.56}Y_{0.05}N$ coating (Fig. 4(b)) maintains its single phase structure at 900 and 1000 °C. The introduction of 5 at.% Y retards the precipitation of *w*-AlN by 100 °C in comparison with $Cr_{0.42}Al_{0.58}N$. *h*-Cr_2N exhibits lower XRD diffraction intensity than that in $Cr_{0.42}Al_{0.58}N$ after annealing at 1100 °C. At 1200 °C, bcc-Cr and fcc-YN are observed, while the original diffraction peaks of cubic phase disappear. Further increasing T_a to 1300 °C, the intensity of bcc-Cr peak becomes more pronounced with the expense of *h*-Cr_2N. Finally, after annealing at 1450 and 1550 °C, $Cr_{0.39}Al_{0.56}Y_{0.05}N$ completely decomposes into *w*-AlN, fcc-YN and bcc-Cr. For $Cr_{0.32}Al_{0.56}Y_{0.12}N$ coating, *w*-AlN is formed during deposition, which also exists with elevating T_a from 900 to 1450 °C (Fig. 4(c)). Likewise, *h*-Cr_2N is generated after annealing at T_a=1100 °C, with a lower intensity than that in $Cr_{0.42}Al_{0.58}N$. The generating temperature of fcc-YN is advanced to 1100 °C due to the increase of Y content. According to previous research, the bonding energy of Y—N (477 kJ/mol) is higher than that of Cr—N (378 kJ/mol) and Al — N (368 kJ/mol) [36]. Besides, ab initio calculations with experiment investigated by ROVERE et al [37] also verified that fcc-YN reveals higher stability than *c*-CrN. Hence, doping with Y effectively stabilizes the N atoms for the Y-containing coatings, especially $Cr_{0.32}Al_{0.56}Y_{0.12}N$. With increasing T_a to 1300 °C, the diffraction intensities of *w*-AlN, *h*-Cr_2N and bcc-Cr continuously increase, suggesting an aggravated

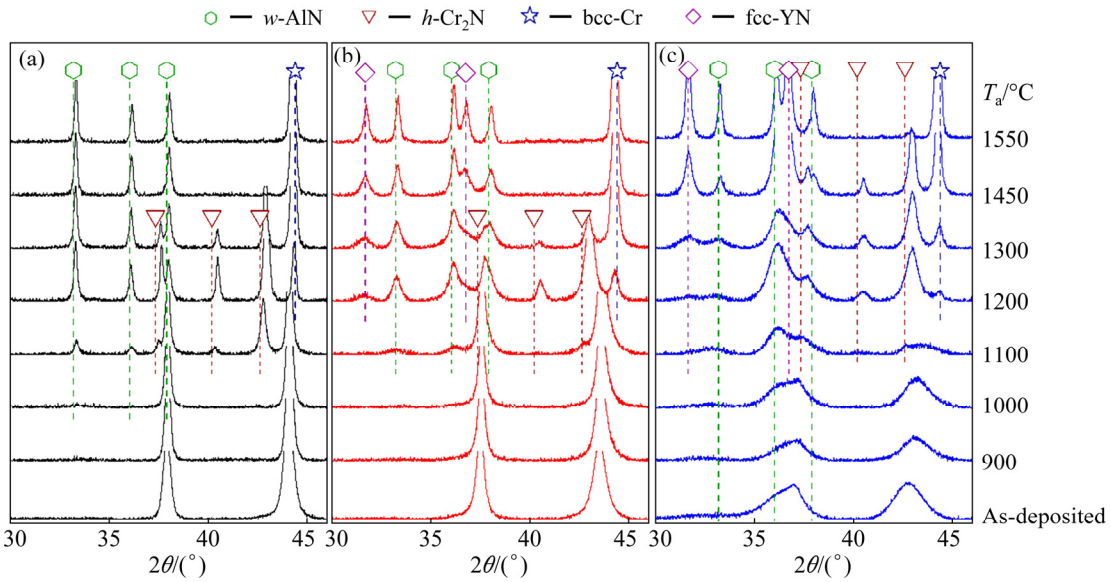

Fig. 4 XRD patterns of $Cr_{0.42}Al_{0.58}N$ (a), $Cr_{0.39}Al_{0.56}Y_{0.05}N$ (b), and $Cr_{0.32}Al_{0.56}Y_{0.12}N$ (c) coatings after annealing up to 1550 °C

thermal decomposition process. After annealing at 1450 °C, the diffraction peaks of *h*-Cr_2N in $Cr_{0.32}Al_{0.56}Y_{0.12}N$ are still prominent, while those in $Cr_{0.42}Al_{0.58}N$ and $Cr_{0.39}Al_{0.56}Y_{0.05}N$ disappear due to the intensified dissociation of Cr—N bonds. Finally, $Cr_{0.32}Al_{0.56}Y_{0.12}N$ coating is composed of *w*-AlN, fcc-YN, *h*-Cr_2N and bcc-Cr at T_a=1550 °C.

The hardness values of coatings during annealing strongly depend on the above-mentioned phase evolution. Figure 5 illustrates the hardness of CrAlN and CrAlYN coatings as a function of annealing temperature. At 900 °C, the annihilation of defects and the relaxation of residual stress lead to a slight reduction in hardness of $Cr_{0.42}Al_{0.58}N$ from (30.2±0.7) GPa in as-deposited state to (28.8±0.9) GPa. The precipitation of *w*-AlN induces a continuous decline of hardness to (27.6±0.8) GPa after annealing at 1000 °C. After annealing at 1100 °C, the hardness of $Cr_{0.42}Al_{0.58}N$ shows a significant decrease to (22.6±0.7) GPa as *h*-Cr_2N is formed and N-loss becomes severe. No distinct variation in the hardness of $Cr_{0.39}Al_{0.56}Y_{0.05}N$ coating is obtained till increasing T_a to 1000 °C. Even after annealing at 1100 °C, $Cr_{0.39}Al_{0.56}Y_{0.05}N$ coating can still maintain a hardness value higher than 31 GPa. $Cr_{0.39}Al_{0.56}Y_{0.05}N$ coating reveals an obvious enhanced ability to maintain its mechanical properties at high temperatures, further verifying the beneficial effect of Y-addition with an amount of 5 at.% on thermal stability. For $Cr_{0.32}Al_{0.56}Y_{0.12}N$ coating, the hardness reaches its peak value of (28.3±0.5) GPa at 900 C. This can be attributed to a more compact microstructure induced by the intensified diffusion process [38], which effectively counteracts negative effects of *w*-AlN formation and recovery process. The hardness of $Cr_{0.32}Al_{0.56}Y_{0.12}N$ can maintain stable after annealing at 1000 °C, owing to the postponed dissociation of Cr—N bonds. However, annealing at 1100 °C leads to a significant drop of hardness to (21.5±0.5) GPa because of the precipitation of *h*-Cr_2N and N-loss.

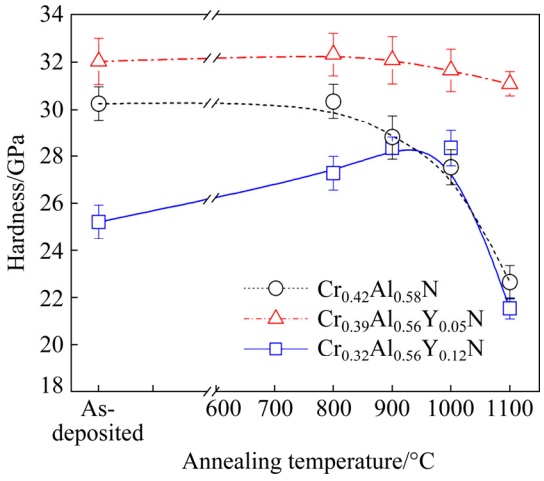

Fig. 5 Hardness of $Cr_{0.42}Al_{0.58}N$, $Cr_{0.39}Al_{0.56}Y_{0.05}N$, and $Cr_{0.32}Al_{0.56}Y_{0.12}N$ coatings as function of annealing temperature T_a

3.4 Oxidation resistance

Figure 6 presents the synchronous TGA and DSC curves from 500 to 1500 °C of $Cr_{0.42}Al_{0.58}N$, $Cr_{0.39}Al_{0.56}Y_{0.05}N$, and $Cr_{0.32}Al_{0.56}Y_{0.12}N$ coatings in synthetic air. Y-incorporation results in an obvious drop in the onset temperature of oxidation, which can be identified by both the starting temperature of exothermic features on DSC curve (Fig. 6(a)) and the initial temperature of mass gain on TGA curve (Fig. 6(b)). By analyzing the data of heat flow, the oxidation process of $Cr_{0.42}Al_{0.58}N$ starts at ~1165 °C, while $Cr_{0.39}Al_{0.56}Y_{0.05}N$ initiates an exothermic feature of oxidation at ~1055 °C. Increasing the Y content to 12 at.% leads to a lower onset temperature of ~780 °C. The TGA curves in Fig. 6(b) also reveal that the onset mass gain temperature of Y-containing coatings is lower than

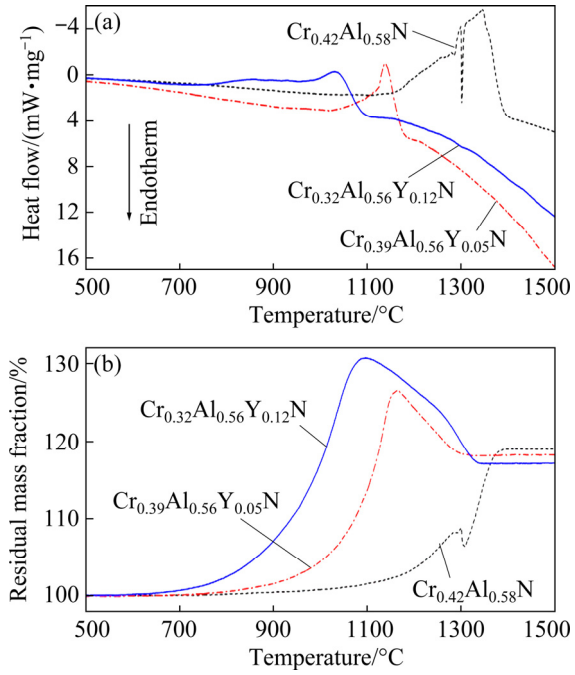

Fig. 6 Simultaneous thermal analysis in synthetic air of $Cr_{0.42}Al_{0.58}N$, $Cr_{0.39}Al_{0.56}Y_{0.05}N$ and $Cr_{0.32}Al_{0.56}Y_{0.12}N$ coatings with temperature up to 1500 °C: (a) TGA; (b) DSC

that of $Cr_{0.42}Al_{0.58}N$, further verifying the negative effect of Y-incorporation on oxidation resistance. It is worth noting that $Cr_{0.39}Al_{0.56}Y_{0.05}N$ and $Cr_{0.32}Al_{0.56}Y_{0.12}N$ coatings both exhibit an extra endotherm feature initiated at ~1180 and ~1090 °C, respectively. This can be ascribed to the dissociation process of Cr—N bonds in CrAlYN coatings, which is endotherm in nature [7]. Besides, the TGA curves of $Cr_{0.39}Al_{0.56}Y_{0.05}N$ and $Cr_{0.32}Al_{0.56}Y_{0.12}N$ begin to show a downtrend at ~1180 and ~1090 °C, respectively, which is consistent with the DSC analysis as the breaking of Cr—N bonds is accompanied with a mass loss [9]. In conclusion, DSC and TGA analyses indicate that alloying with Y exerts an adverse impact on the oxidation resistance of CrAlN coatings.

Figure 7 presents the XRD patterns of $Cr_{0.42}Al_{0.58}N$, $Cr_{0.39}Al_{0.56}Y_{0.05}N$, and $Cr_{0.32}Al_{0.56}Y_{0.12}N$ coatings after oxidation at given temperatures. $Cr_{0.42}Al_{0.58}N$ coating can keep unoxidized at 1000 °C, as shown in Fig. 7(a). After oxidation at 1100 °C, the diffraction peaks of α-Cr_2O_3 (space group $R\bar{3}c$) and/or α-Al_2O_3 (space group $R\bar{3}c$) occur, which are more prominent with elevating T_a to 1200 °C. Increasing T_a to 1300 °C leads to the breaking of Cr—N bonds and N-loss, which is demonstrated by the emergence of h-Cr_2N. After the oxidation at 1400 °C, the original diffraction peaks of cubic phase disappear, and $Cr_{0.42}Al_{0.58}N$ coating is completely oxidized into α-Cr_2O_3, α-Al_2O_3 and their mixed phase α-$(Cr,Al)_2O_3$ (space group $R\bar{3}c$).

For $Cr_{0.39}Al_{0.56}Y_{0.05}N$, α-Cr_2O_3 and α-Al_2O_3 are detected at 1000 °C, indicating that Y-incorporation decreases the onset temperature of oxidation. At 1100 °C, feeble peaks of orthometric structure (o-) $YCrO_3$ (space group *Pnma*) and o-$YAlO_3$ (YAP, space group *Pnma*) are observed. With increasing oxidation temperature to 1200 °C, the original diffraction signals of cubic phase are nearly invisible in $Cr_{0.39}Al_{0.56}Y_{0.05}N$, further manifesting a weakened oxidation resistance. The formation of h-Cr_2N indicates the N-loss process in $Cr_{0.39}Al_{0.56}Y_{0.05}N$, corresponding to its TGA curve in Fig. 6(b) which starts to go down at 1200 °C. In addition, a small amount of cubic (c-) Y_2O_3 (space group $1\bar{a}3$) are detectable in $Cr_{0.39}Al_{0.56}Y_{0.05}N$ after being oxidated at 1200 °C. By further increasing the temperature to 1300 °C, c-Y_2O_3 is not detected as it combines with Cr and/or Al to form the orthometric $YCrO_3$ and/or $YAlO_3$, which mainly aggregates at the grain boundaries for Y-doped coatings [39,40]. Finally, $Cr_{0.39}Al_{0.56}Y_{0.05}N$ is composed of α-$(Cr,Al)_2O_3$, o-$YCrO_3$, o-$YAlO_3$ and h-Cr_2N at 1400 °C. The phase evolution of $Cr_{0.32}Al_{0.56}Y_{0.12}N$ is similar to that of $Cr_{0.39}Al_{0.56}Y_{0.05}N$ except for the existing temperature of c-Y_2O_3 as well as the formation of h-$YAlO_3$ and c-$Y_3Al_5O_{12}$. c-Y_2O_3 can be detected at 1200 and 1300 °C as a higher Y content elevates the temperature where it is fully consumed. Additionally, another $YAlO_3$, designated yttrium aluminum hexagonal (YAH), with space

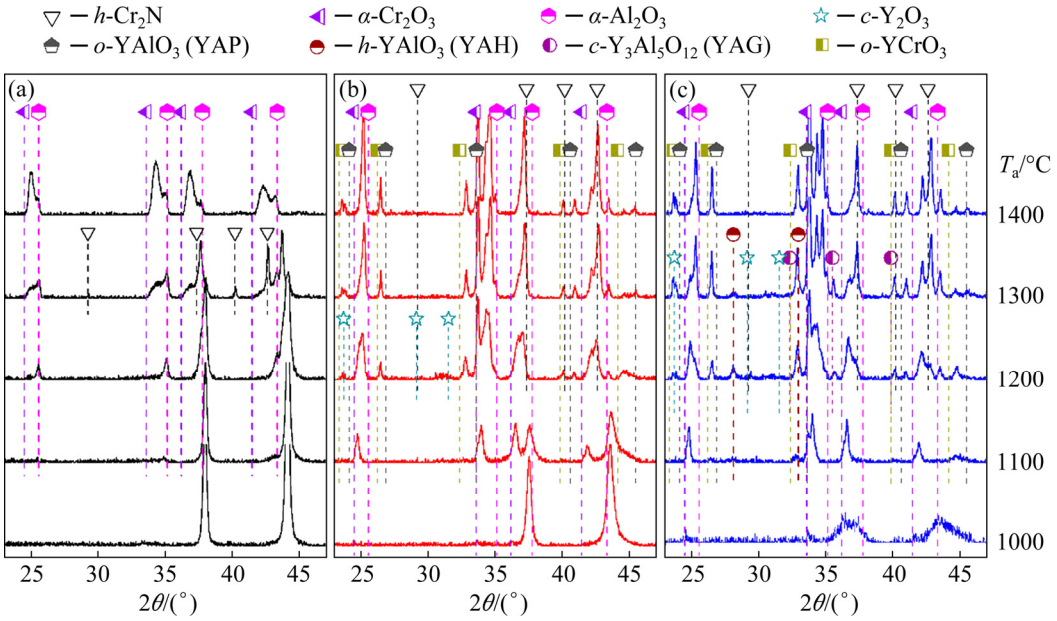

Fig. 7 XRD patterns of $Cr_{0.42}Al_{0.58}N$ (a), $Cr_{0.39}Al_{0.56}Y_{0.05}N$ (b), and $Cr_{0.32}Al_{0.56}Y_{0.12}N$ (c) powdered samples after oxidation in synthetic air up to 1400 °C

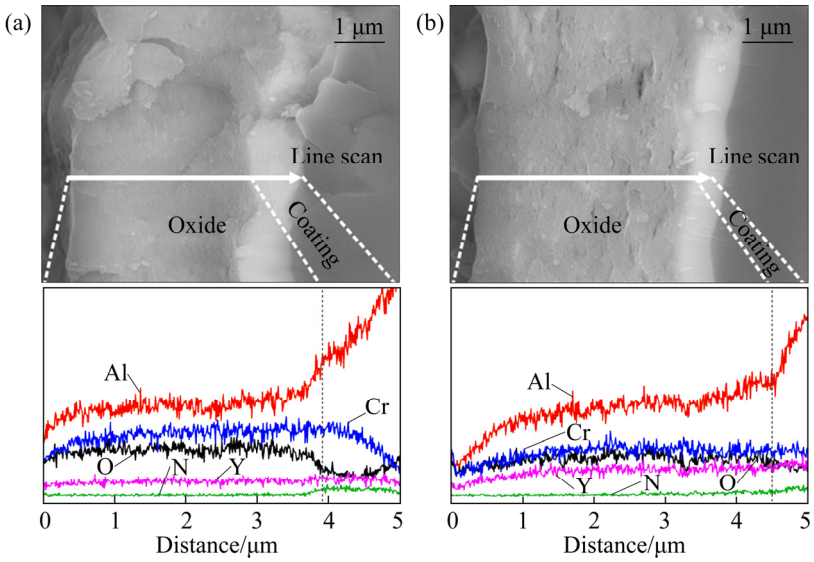

Fig. 8 SEM fracture cross-sectional morphologies and EDX line-scan profiles of $Cr_{0.39}Al_{0.56}Y_{0.05}N$ (a) and $Cr_{0.32}Al_{0.56}Y_{0.12}N$ (b) coatings on polycrystalline Al_2O_3 substrates after isothermal oxidation in synthetic air at 800 °C for 15 h

group of $P6_3/mmc$, occurs at 1100 °C. After oxidation at 1200 °C, $Y_3Al_5O_{12}$ (YAG), with a garnet structure of cubic system (space group $1\bar{a}3d$), emerges with an obvious diffraction peak at ~35.5°, which disappears at 1400 °C. Furthermore, *h*-$YAlO_3$ gradually transforms into *c*-$Y_3Al_5O_{12}$ at 1200 °C, which is also not detectable at 1400 °C [41].

Figure 8 depicts the cross-sectional SEM morphologies and EDX line-scan profiles of $Cr_{0.39}Al_{0.56}Y_{0.05}N$ and $Cr_{0.32}Al_{0.56}Y_{0.12}N$ coatings after isothermal oxidation at 800 °C for 15 h. $Cr_{0.42}Al_{0.58}N$ coating possesses excellent oxidation resistance so that it is not affected after oxidation at 800 °C for 15 h according to the previous report [6]. By contrast, $Cr_{0.39}Al_{0.56}Y_{0.05}N$ (Fig. 8(a)) and $Cr_{0.32}Al_{0.56}Y_{0.12}N$ (Fig. 8(b)) reveal thick oxide scales of ~3.9 and ~4.5 μm, respectively, suggesting that Y-addition reduces the oxidation resistance of CrAlN coatings. EDX line-scan analysis was performed on the oxidized CrAlYN samples to further explore the elemental distribution of the oxide layers. It can be found that the Cr, Al, O, and Y elements are evenly distributed in the oxidized region. The early formation of Y-containing phases including $YCrO_3$, $YAlO_3$ and Y_2O_3 located in grain boundaries provides a fast channel for the inward diffusion of oxygen anions [20], and thus weakens the oxidation resistance of Y-containing coatings. Besides, the oxide layers of $Cr_{0.39}Al_{0.56}Y_{0.05}N$ and $Cr_{0.32}Al_{0.56}Y_{0.12}N$ show a porous structure. Increased thickness of oxide layer with increasing Y-content can be observed by the SEM fracture cross-sectional images and EDX line-scan profiles.

4 Conclusions

(1) $Cr_{0.42}Al_{0.58}N$ and $Cr_{0.39}Al_{0.56}Y_{0.05}N$ coatings both reveal a single phase face-centered cubic structure, but $Cr_{0.32}Al_{0.56}Y_{0.12}N$ presents a cubic−wurtzite mixed structure. The hardness of $Cr_{0.39}Al_{0.56}Y_{0.05}N$ rises to (32.0±1.0) GPa from (30.2±0.7) GPa of $Cr_{0.42}Al_{0.58}N$ owing to the solid solution mechanism and Hall−Petch effect. However, the formation of *w*-AlN in $Cr_{0.32}Al_{0.56}Y_{0.12}N$ leads to a drop in hardness to (25.2±0.7) GPa.

(2) The addition of 5 at.% Y into CrAlN postpones the formation of *w*-AlN by 100 °C compared with $Cr_{0.42}Al_{0.58}N$. In addition, $Cr_{0.39}Al_{0.56}Y_{0.05}N$ coating consistently exhibits the highest hardness value during annealing.

(3) The introduction of Y results in thicker oxide layers of ~3.9 μm for $Cr_{0.39}Al_{0.56}Y_{0.05}N$ and ~4.5 μm for $Cr_{0.32}Al_{0.56}Y_{0.12}N$ after isothermal oxidation at 800 °C for 15 h. Y dramatically weakens the oxidation resistance of CrAlN coating owing to the earlier formation of Y-containing oxide phases ($YCrO_3$, $YAlO_3$ and Y_2O_3) which provides a fast channel for oxygen and then the porous and nonprotective oxide layer is formed.

Acknowledgments

The authors are grateful for the financial supports from the National Natural Science Foundation of China (No. 51775560). Li CHEN thanks the support of the State Key Laboratory of Powder Metallurgy from the Central South University of China.

References

[1] WARCHOLINSKI B, GILEWICZ A, KUPRIN A S, KOLODIY I V. Structure and properties of CrN coatings formed using cathodic arc evaporation in stationary system [J]. Transactions of Nonferrous Metals Society of China, 2019, 29: 799−810.

[2] SHAN Lei, ZHANG Yang-rong, WANG Yong-xin, LI Jin-long, JIANG Xin, CHEN J M. Corrosion and wear behaviors of PVD CrN and CrSiN coatings in seawater [J]. Transactions of Nonferrous Metals Society of China, 2016, 26: 175−184.

[3] DU Jian-wei, CHEN Li, CHEN Jie, DU Yong. Mechanical properties, thermal stability and oxidation resistance of TiN/CrN multilayer coatings [J]. Vacuum, 2020, 179: 109468.

[4] ZHU Li-hui, SONG Cheng, NI Wang-yan, LIU Yi-xiong, Effect of 10% Si addition on cathodic arc evaporated TiAlSiN coatings [J]. Transactions of Nonferrous Metals Society of China, 2016, 26: 1638−1646.

[5] CHEN Li, DU Yong, WANG She-quan, LI Jia. A comparative research on physical and mechanical properties of (Ti,Al)N and (Cr,Al)N PVD coatings with high Al content [J]. International Journal of Refractory Metals and Hard Materials, 2007, 25: 400−404.

[6] YANG Bing, CHEN Li, CHANG Ke-ke, PAN Wei, PENG Ying-biao, DU Yong, LIU Yiu. Thermal and thermo-mechanical properties of Ti−Al−N and Cr−Al−N coatings [J]. International Journal of Refractory Metals and Hard Materials, 2012, 35: 235−240.

[7] HE Lin-qing, CHEN Li, XU Yu-xiang, DU Yong. Thermal stability and oxidation resistance of $Cr_{1-x}Al_xN$ coatings with single phase cubic structure [J]. Journal of Vacuum Science and Technology A, 2015, 33: 061513.

[8] TILLMANN W, KOKALJ D, STANGIER D, PAULUS M, STERNEMANN C, TOLAN M. Investigation on the oxidation behavior of $AlCrV_xN$ thin films by means of synchrotron radiation and influence on the high temperature friction [J]. Applied Surface Science, 2018, 427: 511−521.

[9] HU Chun, XU Yu-xiang, CHEN Li, PEI Fei, DU Yong, Mechanical properties, thermal stability and oxidation resistance of Ta-doped CrAlN coatings [J]. Surface and Coatings Technology, 2019, 368: 25−32.

[10] CHEN Li, LIU Zi-qiang, XU Yu-xiang, DU Yong. Influence of Zr on structure, mechanical and thermal properties of Cr−Al−N coatings [J]. Surface and Coatings Technology, 2015, 275: 289−295.

[11] HE Lin-qing, CHEN Li, XU Yu-xiang. Interfacial structure, mechanical properties and thermal stability of CrAlSiN/CrAlN multilayer coatings [J]. Materials Characterization, 2017, 125: 1−6.

[12] CHANG Chi-lung, HUANG Chi-song, JAO Jui-yun. Microstructural, mechanical and wear properties of Cr−Al−B−N coatings deposited by DC reactive magnetron co-sputtering [J]. Surface and Coatings Technology, 2011, 205: 2730−2737.

[13] XU Yu-xiang, HU Chun, CHEN Li, PEI Fei, DU Yong. Effect of V-addition on the thermal stability and oxidation resistance of CrAlN coatings [J]. Ceramics International, 2018, 44: 7013−7019.

[14] FRANZ R, MITTERER C. Vanadium containing self-adaptive low-friction hard coatings for high-temperature applications: A review [J]. Surface and Coatings Technology, 2013, 228: 1−13.

[15] SÁNCHEZ-LÓPEZ J C, CONTRERAS A, DOMÍNGUEZ-MEISTER S, GARCÍA-LUIS A, BRIZUELA M. Tribological behaviour at high temperature of hard CrAlN coatings doped with Y or Zr [J]. Thin Solid Films, 2014, 550: 413−420.

[16] TRITREMMEL C, DANIEL R, MITTERER C, MAYRHOFER P H, LECHTHALER M, POLCIK P. Oxidation behavior of arc evaporated Al−Cr−Si−N thin films [J]. Journal of Vacuum Science and Technology A, 2012, 30: 061501.

[17] CHEN Yun, DU Hao, CHEN Ming, YANG Jun, XIONG Ji, ZHAO Hai-bo. Structure and wear behavior of AlCrSiN-based coatings [J]. Applied Surface Science, 2016, 370: 176−183.

[18] NOSE M, KAWABATA T, WATANUKI T, UEDA S, FUJII K, MATSUDA K, IKENO S. Mechanical properties and oxidation resistance of CrAlN/BN nanocomposite coatings prepared by reactive dc and rf cosputtering [J]. Surface and Coatings Technology, 2011, 205: s33−s37.

[19] ROVERE F, MAYRHOFER P H, REINHOLDT A, MAYER J, SCHNEIDER J M. The effect of yttrium incorporation on the oxidation resistance of Cr−Al−N coatings [J]. Surface and Coatings Technology, 2008, 202: 5870−5875.

[20] QI Zheng-bing, WU Zheng-tao, WANG Zhou-cheng. Improved hardness and oxidation resistance for CrAlN hard coatings with Y addition by magnetron co-sputtering [J]. Surface and Coatings Technology, 2014, 259: 146−151.

[21] ROVERE F, MAYRHOFER P H. Impact of yttrium on structure and mechanical properties of Cr−Al−N thin films [J]. Journal of Vacuum Science and Technology A, 2007, 25: 1336−1340.

[22] ROVERE F, MAYRHOFER P H. Thermal stability and thermo-mechanical properties of magnetron sputtered Cr−Al−Y−N coatings [J]. Journal of Vacuum Science and Technology A, 2008, 26: 29−35.

[23] ROJAS T C, EL MRABET S, DOMÍNGUEZ-MEISTER S, BRIZUELA M, GARCÍA-LUIS A, SÁNCHEZ-LÓPEZ J C. Chemical and microstructural characterization of (Y or Zr)-doped CrAlN coatings [J]. Surface and Coatings Technology, 2012, 211: 104−110.

[24] MATO S, ALCALÁ G, BRIZUELA M, ESCOBAR GALINDO R, PÉREZ F J, SÁNCHEZ-LÓPEZ J C. Long-term high temperature oxidation of CrAl(Y)N coatings in steam atmosphere [J]. Corrosion Science, 2014, 80:

453−460.
[25] OLIVER W C, PHARR G M. An improved technique for determining hardness and elastic modulus using load and displacement sensing indentation experiments [J]. Journal of Materials Research, 1992, 7: 1564−1583.
[26] PEI Fei, XU Yu-xiang CHEN Li, DU Yong, ZOU Hou-ke. Structure, mechanical properties and thermal stability of $Ti_{1-x}Si_xN$ coatings [J]. Ceramics International, 2018, 44: 15503−15508.
[27] SLATER J C. Atomic radii in crystals [J]. Journal of Chemical Physics, 1964, 41: 3199−3204.
[28] ZHUANG Qi-ming, LIN Nan, HE Yue-hui, KANG Xi-yue. Influence of temperature on sintering behavior and properties of TiC−Fe−Co−Ni−Cr−Mo cermets [J]. Ceramics International, 2017, 43: 15992−15998.
[29] SCHERRER P. Determination of the size and internal structure of colloidal particles using X-480 rays [M]. Math-Phys Kl, Nachr Ges Wiss Goettingen, 1918. (in Germany)
[30] PANJAN P, DRNOVŠEK A, GSELMAN P, ČEKADA M, PANJAN M. Review of growth defects in thin films prepared by PVD techniques [J]. Coatings, 2020, 10: 1−39.
[31] QI Zheng-bing, ZHU Fang-ping, WU Zheng-tao, LIU Bin, WANG Zhou-cheng, PENG Dong-liang, WU Chong-hu. Influence of yttrium addition on microstructure and mechanical properties of ZrN coatings [J]. Surface and Coatings Technology, 2013, 231: 102−106.
[32] ZOU Dong-li, HE Li-feng, XIAO Da-wu, ZHAO Ya-wen, QIU Zhi-chong, LU Chao, LIU Fan. Microstructure and mechanical properties of fine grained uranium prepared by ECAP and subsequent intermediate heat treatment [J]. Transactions of Nonferrous Metals Society of China, 2020, 30: 2749−2756.
[33] KIM H S, BUSH M B. The effects of grain size and porosity on the elastic modulus of nanocrystalline materials [J]. Nanostructured Materials, 1999, 11: 361−367.
[34] HU Chun, XU Yu-xiang, CHEN Li, PEI Fei, ZHANG Li-jun, DU Yong. Structural, mechanical and thermal properties of CrAlNbN coatings [J]. Surface and Coatings Technology, 2018, 349: 894−900.
[35] MAYRHOFER P H, WILLMANN H, REITER A E, Structure and phase evolution of Cr−Al−N coatings during annealing [J]. Surface and Coatings Technology, 2008, 202: 4935−4938.
[36] HAYNES W M, BRUNO T J, LIDE D R. CRC handbook of chemistry and physics [M]. 95th edition. Crc Press, Inc, 2014.
[37] ROVERE F, MUSIC D, SCHNEIDER J M, MAYRHOFER P H. Experimental and computational study on the effect of yttrium on the phase stability of sputtered Cr−Al−Y−N hard coatings [J]. Acta Materialia, 2010, 58: 2708−2715.
[38] WILLMANN H, BECKERS M, GIULIANI F, BIRCH J, MAYRHOFER P H, MITTERER C, HULTMAN L. Single-crystal growth of NaCl-structure Al−Cr−N thin films on MgO(001) by magnetron sputter epitaxy [J]. Scripta Materialia, 2007, 57: 1089−1092.
[39] CAPDEVILA C, PIMENTEL G, ARANDA M M, REMENTERIA R, DAWSON K, URONES-GARROTE E, TATLOCK G J, MILLER M K. Role of Y−Al oxides during extended recovery process of a ferritic ODS alloy [J]. JOM, 2015, 67: 2208−2215.
[40] KARPINOS D M, LISTOVNICHAYA S P, BALAKHNINA V N, OKUNEVSKII Y N. Reaction between thin yttrium oxide and chromium films in the presence of oxygen [J]. Soviet Powder Metallurgy and Metal Ceramics, 1979, 18: 668−671.
[41] SIM S M, KELLER K A, MAH T I. Phase formation in yttrium aluminum garnet powders synthesized by chemical methods [J]. Journal of Materials Science, 2000, 35: 713−717.

Y 掺杂 CrAlN 涂层的结构、力学与热性能

田金莲[1]，胡 春[1]，陈 利[1]，楼玉民[2]，赵宁宁[2]

1. 中南大学 粉末冶金国家重点实验室，长沙 410083；
2. 浙江浙能技术研究院有限公司，杭州 412007

摘 要：采用阴极弧蒸发法制备不同 Y 含量(0、5%和 12%，摩尔分数)的 CrAlYN 涂层，使用 X 射线衍射、扫描电子显微镜、差示扫描量热仪、热重分析仪和纳米压痕技术研究 Y 掺杂对 CrAlN 涂层结构、力学性能以及热性能的影响。$Cr_{0.42}Al_{0.58}N$ 和 $Cr_{0.39}Al_{0.56}Y_{0.05}N$ 涂层为单相立方结构，而 $Cr_{0.32}Al_{0.56}Y_{0.12}$ 涂层为立方−六方混合结构，由于结构的转变，涂层硬度值由 $Cr_{0.42}Al_{0.58}N$ 的(30.2±0.7) GPa 和 $Cr_{0.39}Al_{0.56}Y_{0.05}N$ 的(32.0±1.0) GPa 下降到 $Cr_{0.32}Al_{0.56}Y_{0.12}N$ 的(25.2±0.7) GPa。热退火过程中六方 AlN 相的析出延迟以及 N 损的延迟证明添加 5% Y 能够延缓 CrAlN 涂层的热分解，相应地，$Cr_{0.39}Al_{0.56}Y_{0.05}N$ 涂层在退火过程中始终表现出最高的硬度值。然而，Y 的掺杂对 CrAlN 涂层的抗氧化性产生不利的影响。

关键词：CrAlYN 涂层；阴极弧蒸发；结构演变；硬度；热稳定性；抗氧化性

(Edited by Bing YANG)